

# Negative dysphotopsia: Causes and rationale for prevention and treatment



Jack T. Holladay, MD, MSEE, Michael J. Simpson, PhD

**Purpose:** To determine the cause of negative dysphotopsia using standard ray-tracing techniques and identify the primary and secondary causative factors.

**Setting:** Department of Ophthalmology, Baylor College of Medicine, Houston, Texas, USA.

**Design:** Experimental study.

**Methods:** Zemax ray-tracing software was used to evaluate pseudophakic and phakic eye models to show the location of retinal field images from various visual field objects. Phakic retinal field angles (RFAs) were used as a reference for the perceived field locations for retinal images in pseudophakic eyes.

**Results:** In a nominal acrylic pseudophakic eye model with a 2.5 mm diameter pupil, the maximum RFA from rays refracted by the intraocular lens (IOL) was 85.7 degrees and the minimum

RFA for rays missing the optic of the IOL was 88.3 degrees, leaving a dark gap (shadow) of 2.6 degrees in the extreme temporal field. The width of the shadow was more prominent for a smaller pupil, a larger angle kappa, an equi-biconvex or plano-convex IOL shape, and a smaller axial distance from iris to IOL and with the anterior capsule overlying the nasal IOL. Secondary factors included IOL edge design, material, diameter, decentration, tilt, and aspheric surfaces.

**Conclusions:** Standard ray-tracing techniques showed that a shadow is present when there is a gap between the retinal images formed by rays missing the optic of the IOL and rays refracted by the IOL. Primary and secondary factors independently affected the width and location of the gap (or overlap). The ray tracing also showed a constriction and double retinal imaging in the extreme temporal visual field.

*J Cataract Refract Surg* 2017; 43:263–275 © 2017 ASCRS and ESCRS

Since the original clinical description of negative dysphotopsia,<sup>1</sup> the cause is still controversial and has not been satisfactorily explained.<sup>2</sup> Our purpose is to point out an oversight in a previous article by Holladay et al.<sup>3</sup> and Holladay<sup>4</sup> and to clarify the factors that contribute to negative dysphotopsia. We propose a unifying concept that explains all the current findings for symptoms and treatment based on standard ray tracing.

We will show via ray tracing that the “extreme” peripheral retinal image (above a visual field angle [VFA] of 80 degrees) is formed from 2 optical paths; that is, (1) rays that are refracted by the intraocular lens (IOL) and (2) those that miss the IOL. If there is a gap between these 2 retinal images, it is perceived as a dark shadow and negative dysphotopsia results. The primary and secondary factors that determine the presence of a gap or overlap will be discussed.

## MATERIALS AND METHODS

Zemax ray-tracing software (Radiant Zemax) was used to evaluate pseudophakic model eyes and phakic model eyes. A phakic eye

was used to provide a basis for comparing VFAs and retinal field angles (RFAs).

## Eye Model Specifications

Table 1 shows the nominal values for the phakic eye model and acrylic and silicone pseudophakic eye models. The parameters are based on both the earlier papers by Holladay et al.<sup>3</sup> and Holladay<sup>4</sup> and values for the phakic eye by Liou and Brennan.<sup>5</sup> The radius and conic constant values for the anterior and posterior crystalline lens surfaces were adjusted to make the eye emmetropic and to give an overall profile similar to that of the natural lens. The table includes nodal points and IOL power values calculated by the ray-tracing software. A distant point source was used for ray-tracing evaluations, and the eye was rotated to change the input angle.

Figure 1 shows a horizontal section of the schematic human right eye used for ray-tracing modeling. The cornea and retina are identical for all 3 eye models (phakic, acrylic pseudophakic, and silicone pseudophakic), and the location of the fovea is the same for all eyes at a 5.0 degrees angle to the posterior pole (optical axis) in the temporal direction. This is also known as angle alpha ( $\alpha$ ), which is the angle between the visual and optical axes of the eye. A nominal 2.5-degree angle kappa ( $\kappa$ )<sup>6</sup> was created by decentrating the pupil nasally by 0.17 mm. (See sixth paragraph of

Submitted: August 5, 2016 | Final revision submitted: November 18, 2016 | Accepted: November 20, 2016

From the Department of Ophthalmology (Holladay), Baylor College of Medicine, Houston, and Optics R&D Consultant (Simpson), Simpson Optics, Arlington, Texas, USA.

Corresponding author: Jack T. Holladay, MD, MSEE, 5108 Braeburn Drive, Bellaire, Texas 77401-4902, USA. E-mail: [holladay@docholladay.com](mailto:holladay@docholladay.com).

Table 1. Nominal values for phakic, acrylic and silicone pseudophakic eye models.

Parameter*	Phakic Eye Model	Pseudophakic Eye Model	
		Acrylic IOL	Silicone IOL
Corneal front surface radius	7.76	7.76	7.76
Corneal front surface Q-value	-0.26	-0.26	-0.26
Corneal index of refraction @ 555 nm	1.376	1.376	1.376
Corneal thickness	0.55	0.55	0.55
Corneal back surface radius	6.36	6.36	6.36
Corneal back surface Q-value	-0.24	-0.24	-0.24
Pupil plane	3.60	4.00	4.00
Lens front surface vertex	3.60	4.50	4.50
Lens front surface radius	9.92	19.69	11.05
Lens front surface Q-value	+2.5	0.00	0.00
Lens index of refraction @ 555 nm	Grad A and Grad P <sup>†</sup>	1.550	1.460
Lens thickness	4.02	0.66	1.03
Lens posterior surface vertex	7.62	5.16	5.53
Lens posterior surface radius	-6.48	-19.69	-11.05
Lens posterior surface Q-value	+0.50	0.00	0.00
Lens equivalent power	23.69	21.74	22.35
Lens diameter (full optic to edge)	9.5	6.00	6.00
Primary nodal point (N <sub>1</sub> )	7.039	6.778	6.819
Secondary nodal point (N <sub>2</sub> )	7.321	7.036	7.069
Axial length	23.5	23.5	23.5

Grad = gradient refractive index values for anterior and posterior crystalline lens from Liou and Brennan model<sup>5</sup>

\*All values in millimeters, with axial distances from anterior corneal vertex and angle  $\kappa = +2.5^\circ$

<sup>†</sup>Air index of refraction = 1.000; tear, aqueous, and vitreous index = 1.336

**Discussion about angle  $\kappa$ .** There are important differences between the phakic model and pseudophakic models. For the phakic model the pupil and anterior vertex of the crystalline lens are at 3.6 mm, whereas for the pseudophakic models the pupil is at 4.0 mm and the anterior vertex of the IOL is at 4.5 mm. The thickness of the crystalline lens is 4.02 mm, but the acrylic IOL and silicone IOL have a thickness of 0.66 mm and 1.03 mm, respectively. The IOLs are nominally equi-biconvex, with a 0.2 mm edge thickness, and the equivalent power was determined so that the paraxial image is in focus (emmetropia) when the anterior surface is positioned at the specified distance from the cornea.

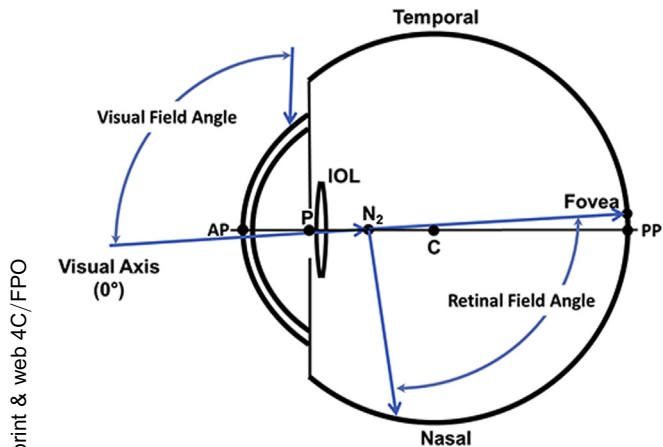
The crystalline lens equivalent power (23.69 diopters [D]) is 1.95 D stronger than the acrylic IOL and 1.34 D stronger than the silicone IOL. This is because of the difference in the index of refraction, the thickness, and that the more posterior location of the posterior surface of the phakic lens leads to a greater effective power for emmetropia. The secondary nodal point for the phakic eye is 16.179 mm from the retina, compared with 16.464 mm for the acrylic IOL eye, which would result in a 1.8% image magnification in pseudophakia with acrylic material compared with the phakic eye.

### Visual Field and Retinal Field Angles

Input VFAs in object space are measured relative to the visual axis, which is defined as zero degrees. Figure 1 shows this angle. In contrast, previous calculations measured angles to the optical axis, which joins the anterior pole and the posterior pole for a

circularly symmetric eye model.<sup>3</sup> Retinal locations are specified here using RFAs, which are measured from the secondary nodal point of the phakic eye (16.179 mm from the retina and 7.321 mm from the corneal vertex (Figure 1), using the visual axis as the zero reference angle. This also differs from earlier studies that used the optical axis as the reference. The relationship between the RFAs and VFAs for the phakic model eye was calculated using the chief ray that goes through the center of the pupil, and this is plotted as the green lines in Figure 2. This is remarkably linear over a very large range of angles, and the 1:1 correspondence is a consequence of using the nodal points as a reference. This provides a one-to-one method for relating retinal locations to their corresponding visual angles for the phakic and pseudophakic eye. The RFA allows these image locations to be compared, and the 1:1 relationship to input VFAs in Figure 2 for the phakic eye then enables these results to be used directly for “apparent” VFA in the pseudophakic eye. The RFA in the pseudophakic eye corresponds to the “apparent” VFA, despite the VFA from which it actually originated.

The ray-tracing phakic eye model could only calculate values to 94 degrees so the remaining values for the green lines in Figure 2 were manually calculated to the measured nominal maximum human temporal VFA of 109 degrees.<sup>7,8</sup> This maximum angle corresponds to a nominal angular deviation by the cornea of 14 degrees for rays at large angles; thus, a ray must be slightly less than 90 degrees to the optical axis at the pupil to enter the pupil. Adding an



print & web 4C/FPO

**Figure 1.** Parameters used for the nominal model eyes. Drawing of right eye from above (AP-N<sub>2</sub> = anterior pole to phakic secondary nodal point = 7.321 mm; AP-P = anterior pole to pupil (external anterior chamber depth) = 4.0 mm; AP-PP = axial length = 23.5 mm (anterior pole to posterior pole); C-PP = center of retinal sphere = 12.0 mm; P-IOL = pupil to anterior vertex of intraocular lens = 0.5 mm)

additional 5 degrees for the angle between the optical axis and the visual axis, the maximum VFA in this study's phakic model is 14 degrees + 90 degrees + 5 degrees = 109 degrees, which matches the measured value.

Calculations were then made for the acrylic pseudophakic eye (2.5 mm and 5.0 mm pupils), determining the maximum RFA for a given VFA for rays refracted by the IOL (blue curves) and minimum RFA for a given VFA for rays missing the optic of the IOL (red curves) shown in Figure 2. The same reference point (phakic N<sub>2</sub>) was used for all RFAs to give the same scaling for retinal locations.

For the 2.5 mm pupil, the blue curve has excellent 1:1 agreement with the phakic eye up to a VFA of 83.8 degrees but then becomes compressed with a cusp and a reversal of the curve with a maximum RFA of 85.7 degrees. These characteristics are a consequence of light no longer being properly focused by the IOL at large visual angles, which is distinctly different from the phakic

eye.<sup>9,10</sup> The acrylic equi-biconvex pseudophakic VFA and RFA limits are primarily a result of the anterior vertex of the IOL being more posterior in the eye than in the young crystalline lens (4.5 mm versus 3.6 mm) and a much smaller optic diameter (6.0 mm versus 9.5 mm).<sup>11,12</sup> The red line shows the VFA versus RFA for the rays missing the optic of the IOL (Figure 2).

For the 5.0 mm pupil, the blue curve deviates slightly more above the green line because the maximum RFA refracted by the IOL has a larger pencil of light entering the larger pupil (Figure 2). The maximum refracted RFA increases to 91.2 degrees (5.5 degrees larger than the 2.5 mm pupil) and corresponds to a similar VFA of 92.1 degrees. The red curve shows the RFA versus VFA for rays missing the optic of the IOL and extends to a much lower minimum VFA of 41.6 degrees due to the larger pupil. Figure 3 shows the limits of the ray tracing for the phakic eyes and pseudophakic eyes for both pupil sizes.

**Ray-Tracing Calculations**

In the ray-tracing simulations, only the horizontal section was used so as to illustrate the optical effects in the temporal visual field. Rays were traced to determine (1) the maximum angle at which a ray could pass through both the pupil and posterior nasal surface of the IOL and (2) the minimum angle at which a ray could pass through the pupil but miss the edge of the IOL. The VFAs and RFAs were recorded for all conditions.

In contrast, Figure 3, A, green area, shows the limiting rays that enter 2.5 mm and 5.0 mm pupils for the phakic eye model. All green rays that enter the pupil pass through the crystalline lens because the iris is draped snugly against the anterior lens capsule and no rays miss the lens. The range is continuous from 0 degree (visual axis) to a nominal maximum VFA and RFA of 109 degrees (green area).

The limiting rays refracted by the IOL (Figure 3, B, blue area) and missing the optic of the IOL (Figure 3, C, red area) are shown for the acrylic pseudophakic model with a 2.5 mm pupil and 5.0 mm pupil. There is a slight gap of -2.6 degrees between the maximum limiting RFA (85.7 degrees) refracted by the IOL and the minimum limiting RFA (88.3 degrees) that misses the IOL for the 2.5 mm pupil. This gap indicates that the temporal field would have a small shadow for the nominal parameters. In this study's model, the missing rays (Figure 3, C) would range from a VFA of 83.8 degrees to 109 degrees, which would correspond

print & web 4C/FPO

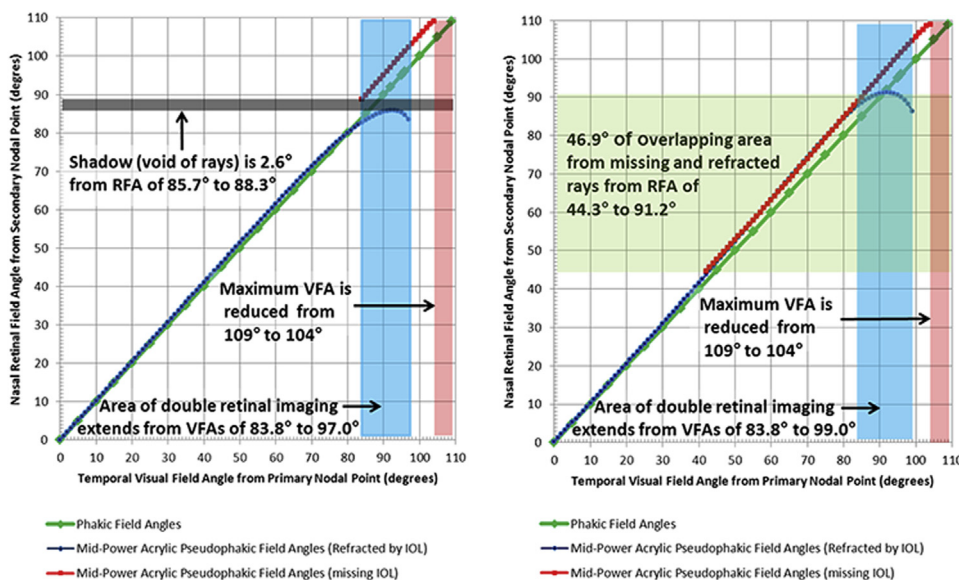
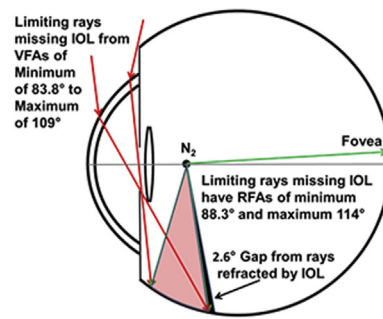
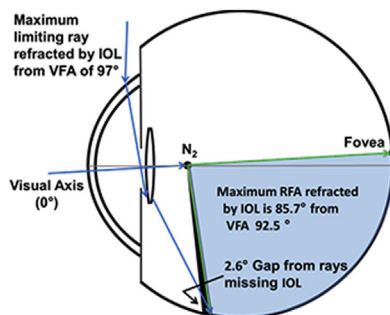
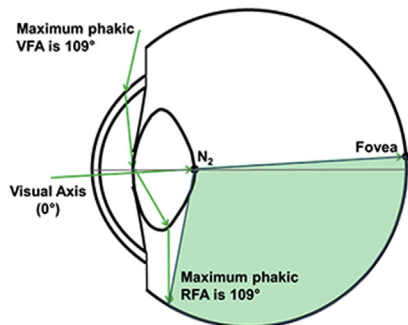
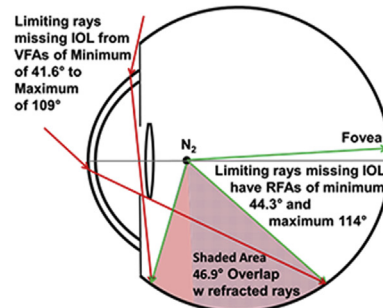
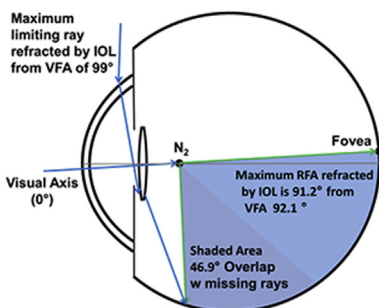
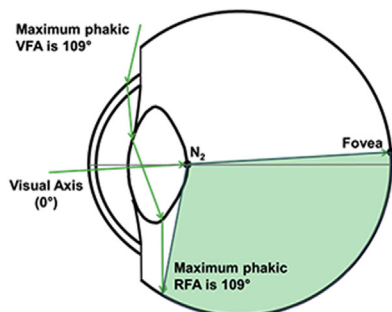


**Figure 2.** For 2.5 mm and 5.0 mm pupils, the green curves demonstrate the equivalency of the VFA and RFA in the phakic model from 0 to 109 degrees. For the 2.5 mm pupil (left) and the acrylic equi-biconvex pseudophakic model, the VFA and RFA for rays refracted by the IOL (blue curve) are equivalent up to 75 degrees, but the maximum VFA is reduced to 97 degrees corresponding to an even smaller RFA of 83.3 degrees. The maximum RFA is 85.7 degrees, which corresponds to a VFA of 92.5 degrees. The rays that miss the IOL (red curve) range from 88.3 to 104 degrees, leaving a gap (shadow) of 2.6 degrees (gray area). For the 5.0 mm pupil (right), the range of rays missing the IOL increases significantly, resulting in a 46.9-degree overlap in the retinal images (green area) (IOL = intraocular lens; RFA = retinal field angle; VFA = visual field angle).

## 2.5 mm pupil



## 5.0 mm pupil



A

B

C

**Figure 3.** Limiting rays for 3 situations (A) phakic (B), pseudophakic maximum refracted rays by IOL, and (C) pseudophakic minimum and maximum rays missing IOL (IOL = intraocular lens; RFA = retinal field angle; VFA = visual field angle).

to an RFA of 88.3 to 114 degrees (although in the phakic eye, the maximum RFA is 109 degrees, which represents the limit of functional retina in the model). For the 5.0 mm pupil in Figure 3, C, there is a 46.9-degree overlap (RFA from 44.3 to 91.2 degrees) of the rays refracted by the IOL and those that miss the IOL, indicating that no shadow is present. The rays that miss the IOL could occur even when the IOL apex is at the pupillary plane if the front surface is convex (not plano) because there is a sagittal drop from the posterior nasal edge of the pupil to the anterior surface of the IOL. The nasal space between the iris and the IOL also increases the more the pupil is decentered nasally from the optical axis.

Two additional important anatomic parameters that are varied in the ray-tracing calculations are the axial separation between the iris and the IOL and angle  $\kappa$ . The axial separation and angle  $\kappa$  affect the limiting rays refracted by and missing the optic of the IOL (Figure 4A and 4B). Actual pupil diameters of 2.5 mm and 5.0 mm were used for the calculations, which correspond to apparent entrance pupils seen by the clinician of 2.86 mm and 5.73 mm diameter (14.5% magnification by cornea). The small pupil and large pupil were used to show the clinical finding that negative dysphotopsia is visible for small pupils only and the effect disappears as the pupil diameter increases.<sup>2</sup>

## RESULTS

### Decentration of Pupil (Angle $\kappa$ ) and Axial Location of the Intraocular Lens

For the nominal equi-biconvex acrylic IOL summarized in Table 1, the graphs in Figures 4A and 4B were generated for a 2.5 and 5.0 mm pupil for 4 conditions: (1) angle  $\kappa = +5.0$  degrees with pupil centered on optical axis, (2) angle  $\kappa = +2.5$  degrees, near the mean for emmetropia, (3) angle

$\kappa = 0.0$  degree with pupil centered on visual axis, and (4) angle  $\kappa = -2.5$  degrees. Angle  $\kappa$ 's were implemented as actual nasal pupil decentration to the optical axis of 0.0, 0.17, 0.34, and 0.5 mm, respectively. For the graphs in Figures 4A and 4B, the  $x$ -axis is the axial distance of the anterior vertex of the IOL behind the iris and the  $y$ -axis is the RFA subtended by the retinal intersecting ray determined using Snell's Law. The blue points are the most anterior rays refracted by the IOL, which have the most anterior retinal intersection, and they indicate the maximum limiting ray angles refracted by the IOL. These rays would originate at very large VFAs and are limited by the temporal edge of the pupil and posterior nasal edge of the IOL. The red points are for the minimum limiting rays that just miss the IOL, which have the most posterior retinal intersection. These rays would typically originate from smaller VFAs, and they represent the ray that would just graze the nasal pupil and nasal edge of the IOL. The gray-shaded areas in Figure 4A indicate the region of negative dysphotopsia for each angle  $\kappa$  as a function of the RFA and the axial distance of IOL behind the iris for the 2.5 mm pupil. The purple-shaded areas in Figure 4B indicate the region of overlap for each angle  $\kappa$  as a function of the RFA and the axial distance of IOL behind the iris for the 5.0 mm pupil, leaving no shadow.

In Figure 4A, the maximum axial distance and area for negative dysphotopsia decrease as angle  $\kappa$  decreases. Notice that the curve for the missing rays (red) is almost linear

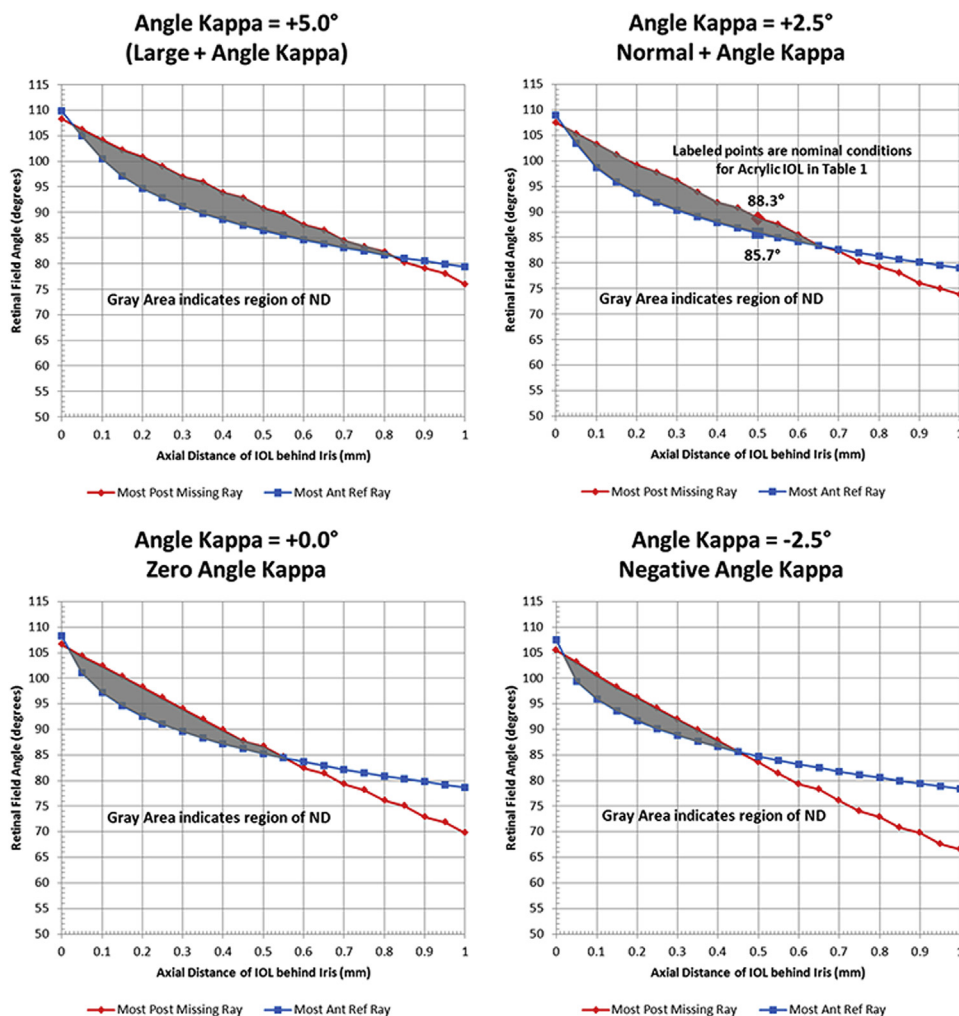


**Figure 4A.** Variation in the gap or shadow (gray area) as a function of angle  $\kappa$  versus axial distance of IOL behind iris for a 2.5 mm pupil (Ant = anterior; IOL = intraocular lens; ND = negative dysphotopsia; Post = posterior).

(straight line) as a function of the RFA and axial space behind the iris, whereas the plot of the refracted rays (blue) is curvilinear with steeper slopes for small axial spaces and flatter slopes for larger, and both depend on angle  $\kappa$ .

For a small photopic pupil, angle  $\kappa$  and the axial separation between the iris and IOL are predominant factors determining the presence of a gap or overlap of the limiting rays refracted by the IOL and those missing the optic of the IOL. The cause of this sensitivity to the pupil can be seen in Figure 3, B and C, for the 2.5 mm pupil, where the rays that miss the IOL are limited directly by the pupil. For larger pupils, light from much smaller visual angles can bypass the IOL and illuminate lower RFAs, resulting in no gap and no perceived shadow.

### Shape and Material of Intraocular Lenses

Another important primary factor determining the location of the limiting anterior pseudophakic ray is the shape of the IOL. Figure 5 shows rays from a large VFA (80 degrees) passing through emmetropic IOLs with different shapes (convex-plano, equi-biconvex, and plano-convex) that all have their anterior vertex at the same location. As the ray tracing and the drawing show, the convex-plano IOL has the shortest focus that is farthest from the retina, followed

by the equi-biconvex and then the plano-convex, which has the longest focus that is nearest the retina. The convex-plano IOL has the greatest spread because it is the most out of focus. The focus in the periphery is not critical because of the poor resolution of the retina in the periphery; however, the convex-plano IOL with the greatest spread also has the most anterior maximum limiting ray refracted by the IOL and therefore the smallest chance for negative dysphotopsia with all other factors equal.

Table 2 shows the limiting VFAs and RFAs along with additional details, including the size of the gap (negative) or overlap (positive) in degrees of RFA (last row). The parameters affecting the gap or overlap from 3 differently shaped IOLs are given for 2 different locations for the axial position of the IOL. In columns 2, 3, and 4, the condition with all 3 shapes of IOLs with their anterior vertex at 0.500 mm is shown for the nominal conditions, which correspond to the IOL locations in Figure 5. In the last row, the convex-plano IOL has a +5.4-degree overlap (no negative dysphotopsia) of the refracted and missing rays whereas there are gaps of -2.6 and -6.1 degrees for the equi-biconvex and plano-convex IOLs, respectively. In columns 5, 6, and 7, a second condition is shown, with the anterior edge of the 3 acrylic IOLs at

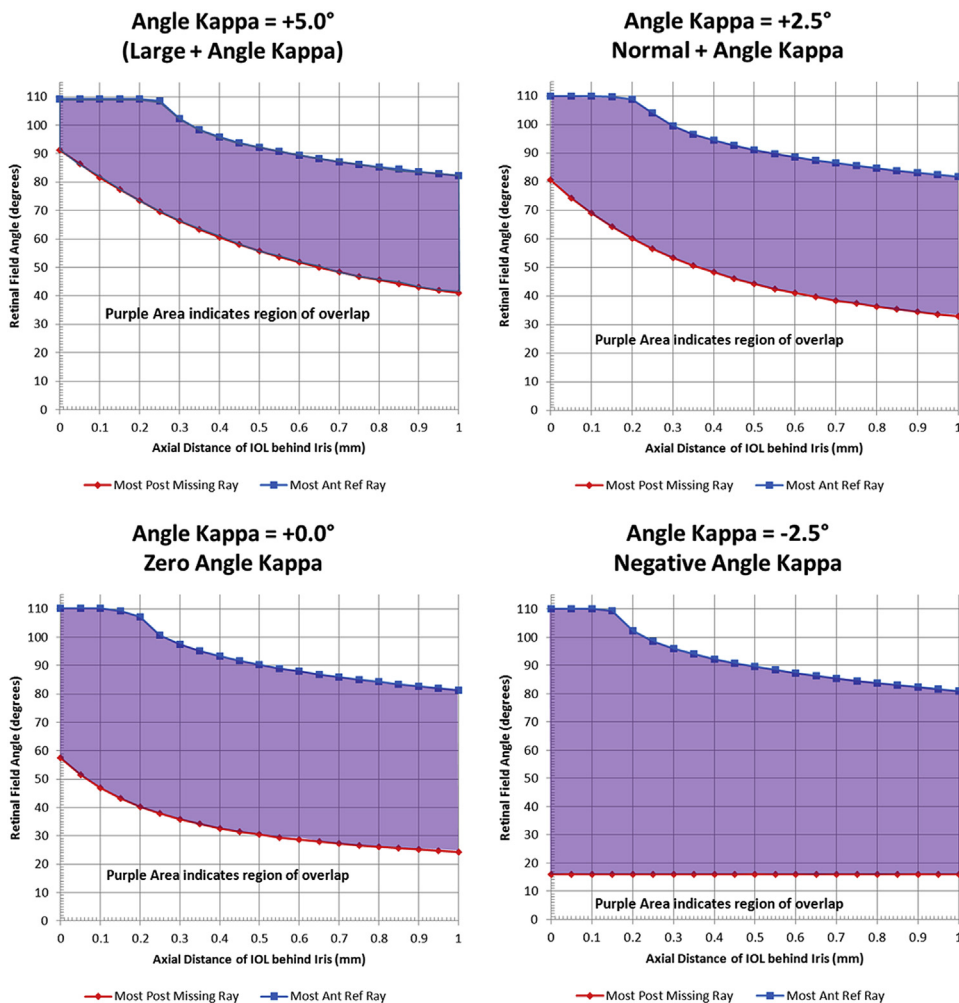


**Figure 4B.** Variation in the overlap (purple area) as a function of angle  $\kappa$  versus axial distance of IOL behind iris for a 5.0 mm pupil (Ant = anterior; IOL = intraocular lens; Post = posterior).

print & web 4C/FPO

the same position as the original equi-biconvex IOL (0.73 mm), making the minimum limiting missing ray for each IOL identical so that the only difference is the maximum refracted ray for each IOL. This comparison isolates the change specifically to the shape of the IOL and shows that the equi-biconvex shape has the greatest gap (−2.6 degrees) with all other factors equal and would have the highest risk for negative dysphotopsia.

In the last 3 columns (8, 9, and 10) in Table 2 the material is changed to a 1.46 refractive index value, like a silicone or low index acrylic IOL, with the anterior edge of the 3 differently shaped IOLs at 0.73 mm (same as the acrylic). The maximum refracted VFA is similar to the acrylic IOLs, but the maximum refracted RFA for the convex-plano IOL is approximately 14.2 degrees higher making the overlap +19.7 degrees. The silicone equi-biconvex has a gap

print & web 4C/FPO

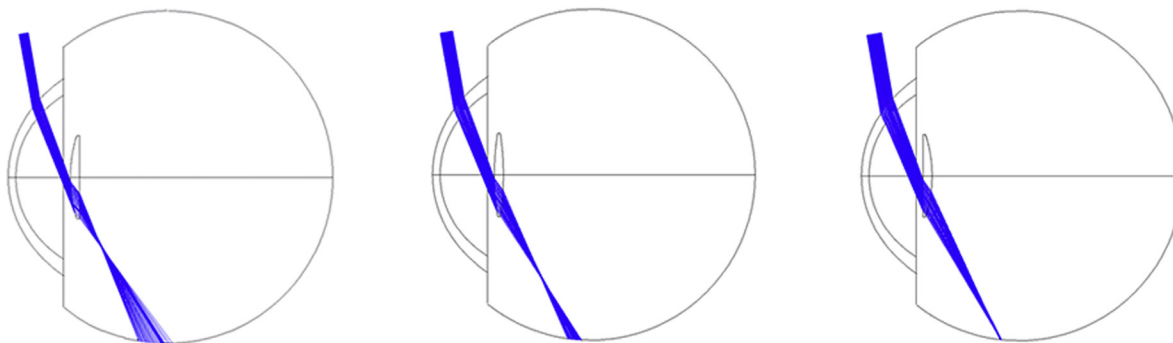


**Figure 5.** The shape of the IOL also has a significant effect on the focus and consequent spread of limiting rays refracted by the IOL on the retina. The VFA is 80 degrees, and the nominal conditions for the acrylic IOL are in columns 2, 3, and 4 of Table 2. The convex-plano IOL (left) has the shortest focus and consequently the greatest spread of RFAs. The plano-convex IOL (right) has the longest focus and the least spread of RFAs, with the equi-biconvex (middle) in between.

Table 2. Effect of shape and material of IOL on shadow.

Parameter	Anterior Vertex of IOL @ 0.500 mm			Anterior Edge of IOL @ 0.730 mm					
	Acrylic			Acrylic			Silicone		
	Convex-Plano	Equi-Biconvex	Plano-Convex	Convex-Plano	Equi-Biconvex	Plano-Convex	Convex-Plano	Equi-Biconvex	Plano-Convex
Power (D)	21.19	21.69	22.29	20.74	21.69	22.83	21.19	22.00	24.22
Anterior vertex (mm)	0.500	0.500	0.500	0.274	0.500	0.730	-0.062	0.322	0.730
Anterior edge (mm)	0.956	0.730	0.500	0.730	0.730	0.730	0.730	0.730	0.730
Edge thickness (mm)	0.204	0.200	0.179	0.200	0.200	0.200	0.200	0.200	0.200
Center thickness (mm)	0.660	0.660	0.660	0.646	0.660	0.693	0.992	1.016	1.171
Sag1 (mm)	0.456	0.230	0.000	0.446	0.230	0.000	0.792	0.408	0.000
Sag2 (mm)	0.000	0.230	0.481	0.000	0.230	0.493	0.000	0.408	0.971
Max ref VFA (°)	89.1	92.5	100.5	93.9	92.5	96.3	92.1	94.5	96.0
Max ref RFA (°)	86.19	85.7	90.2	93.8	85.7	88.9	108.0	87.9	88.5
Min miss VFA (°)	76.7	83.8	91.5	83.8	83.8	83.8	83.8	83.8	83.8
Min miss RFA (°)	80.8	88.3	96.3	88.3	88.3	88.3	88.3	88.3	88.3
Ref-miss RFA* (°)	+5.4	-2.6 <sup>†</sup>	-6.1 <sup>†</sup>	+5.5	-2.6 <sup>†</sup>	+0.6	+19.7	-0.4 <sup>†</sup>	+0.2

IOL = intraocular lens; miss = missing; Ref = refracted; Ref-miss = refracted minus missing; RFA = retinal field angle; Sag = sagittal; VFA = visual field angle

\*Negative sign indicates "gap" or shadow; positive sign indicates overlap

<sup>†</sup>Shadow

that is 2.2 degrees less than the acrylic but is still slightly negative (-0.4 degrees) and the silicone plano-convex is almost identical.

Table 3 shows the effect of power for each IOL shape. The low, mid, and high equi-biconvex powers are 10.0 D, 21.69 D, and 30.0 D, respectively. The powers for the convex-plano and plano-convex have the same paraxial focus as the respective equi-biconvex. For the equi-biconvex and the plano-convex, the last row decreases as the IOL power increases (more gap or less overlap). In contrast, the convex-plano increases the overlap with the increase in IOL power. Figure 5 shows the cause. The short focus of the convex-plano IOL becomes even shorter with increasing power causing the fan of rays to spread even more, resulting in a maximum RFA of 108.4 degrees and an overlap of 20.1 degrees.

#### Effect of Anterior Capsule Overlapping the Intraocular Lens

The maximum limiting rays refracted by the IOL strike the anterior surface of the IOL within a few hundredths of a millimeter from the anterior edge, at incident angles that are just less than 90 degrees. Reflection values are plotted in Figure 6 as a function of incident angle for both IOL materials and the lens capsule. The amount of light reflected at these large angles would be in excess of 90%, leaving less than 10% actually transmitted to the retina. If the nasal portion of the IOL were covered by anterior capsule, with reflections at both the anterior and posterior surfaces of the capsule, the transmitted intensity would be greatly reduced. The reduction in intensity would be similar at

both the front surface and back surface of the anterior capsule, resulting in less than 1% of the light actually incident on the anterior IOL. The anterior capsule would therefore serve as an additional factor, significantly reducing the intensity of the maximum limiting refracted ray.

#### Secondary Factors

The ray-tracing analysis showed that edge design (truncated versus rounded and edge thickness), optic diameter, decentration/tilt of IOL, and aspheric surface(s) are secondary factors that affect the gap or overlap by less than a few degrees of RFA. The material, asphericity of the surface(s), and truncated or rounded edge design, only affect the maximum refracted rays (no effect on the rays missing the optic of the IOL). The diameter, decentration/tilt, and edge thickness of the IOL move the refracted and missing rays similarly so the effect on the gap (or overlap) is minimal, making their impact on negative dysphotopsia even less.

The introduction of aspheric surfaces adds another level of complexity to the ray tracing. Aspheric IOLs are intended to reduce the positive spherical aberration of the cornea, which is nominally +0.27  $\mu\text{m}$  over a 6.0 mm zone, with current aspheric IOLs ranging from 0.00  $\mu\text{m}$  to -0.27  $\mu\text{m}$ . The result of negative asphericity in the IOL surface is a progressive reduction in the curvature (power) of the IOL surface moving toward the periphery of up to approximately 1.5 D. The reduction in peripheral power would reduce the maximum limiting refracted ray by the IOL to a smaller RFA; however, the exact amount would depend on the amount of asphericity, the shape and power of the IOL, and the surface(s) used. The overall effect of

Table 3. Acrylic IOL with low, mid, and high dioptric powers with anterior edge of IOL @ 0.730 mm.

Parameter	Convex-Plano			Equi-Biconvex			Plano-Convex		
	Low	Mid	High	Low	Mid	High	Low	Mid	High
Power (D)	9.77	20.74	28.10	10.00	21.69	30.00	10.24	22.83	32.30
Anterior vertex (mm)	0.524	0.274	0.114	0.625	0.500	0.410	0.730	0.730	0.730
Anterior edge (mm)	0.730	0.730	0.730	0.730	0.730	0.730	0.730	0.730	0.730
Edge thickness (mm)	0.200	0.200	0.200	0.200	0.200	0.200	0.200	0.200	0.200
Center thickness (mm)	0.407	0.646	0.817	0.410	0.660	0.840	0.417	0.693	0.918
Sag1 (mm)	0.206	0.446	0.616	0.105	0.230	0.320	0.000	0.000	0.000
Sag2 (mm)	0.000	0.000	0.000	0.105	0.230	0.320	0.216	0.493	0.718
Max ref VFA (°)	93.6	93.9	105.0	96.7	92.5	91.7	96.3	96.3	96.3
Max ref RFA (°)	90.6	93.8	108.4	90.4	85.7	84.3	91.8	88.9	85.4
Min miss VFA (°)	83.8	83.8	83.8	83.8	83.8	83.8	83.8	83.8	83.8
Min miss RFA (°)	88.3	88.3	88.3	88.3	88.3	88.3	88.3	88.3	88.3
Ref-miss RFA* (°)	+2.3	+5.5	+20.1	+2.1	-2.6 <sup>†</sup>	-4.0 <sup>†</sup>	+3.5	+0.6	-2.9 <sup>†</sup>

IOL = intraocular lens; miss = missing; Ref = refracted; Ref-miss = refracted minus missing; RFA = retinal field angle; Sag = sagittal; VFA = visual field angle

\*Negative sign indicates "gap" with negative dysphotopsia; positive sign indicates overlap

<sup>†</sup>Negative dysphotopsia

negative asphericity would be to reduce the maximum refracted ray by the IOL and slightly increase the risk for negative dysphotopsia proportional to the amount of negative spherical aberration in the IOL.

## DISCUSSION

In the article by Holladay et al.,<sup>3</sup> a type 3 shadow, which was defined as the shadow region between rays that pass through the periphery of the posterior optical surface and rays that pass through the actual edge of the IOL, was concluded to be the cause of negative dysphotopsia. For the 2.5 mm pupil in their Table 1, the ray forming the anterior border of the type 3 shadow on the retina originates from an angle of 81.0 degrees and the posterior ray from 93.4 degrees to the optical axis. However, only pencils of rays from the limiting angles were used. In our Figure 3 (B in top and bottom rows), the rays refracted by the IOL are not limited to a minimum of 81.0 degrees but extend all the way back to the fovea (0 degree). When these rays from smaller angles are added, they completely cover the type 3 shadow, as shown in Figure 7 (light blue area). If all the rays entering the pupil were used, as in natural conditions, there would be no shadow from this cause.

Our ray tracing indicates that the primary factors determining the presence of a temporal shadow are smaller photopic pupil, higher angle  $\kappa$ , equi-biconvex shape with higher power of IOL, smaller axial location, and nasal anterior capsule overlying anterior IOL (Figure 8). It is almost impossible clinically to know whether the nasal anterior capsule is contributing to negative dysphotopsia; however, there is very little risk in removal with the laser, and 60% improvement has been reported with both plate-haptic and looped-

haptic posterior chamber in-the-bag IOLs.<sup>13-15</sup> A recent article by Makhotkina et al.<sup>16</sup> corroborates our finding that for equi-biconvex IOLs, the risk for negative dysphotopsia increases with higher IOL powers. However, higher IOL powers are also associated with hyperopia, which is also associated with higher angle  $\kappa$ 's<sup>6</sup> and smaller pupils,<sup>17,18</sup> which independently are primary causative factors of negative dysphotopsia.

Secondary factors include IOL edge design (rounded or truncated) and edge thickness, material, diameter, tilt/decentration, and negative asphericity of 1 or both surfaces. When the gap between the rays refracted and missing the IOL is small (1 or 2 degrees), the patient might perceive the shadow as a dark vertical line. For larger gaps, they would report a dark crescent-shaped shadow as in the patient drawings in Figure 9.

Figure 10 shows simulated retinal images of shadows with a varying width and temporal location for a 2.5 mm pupil. The central image represents the nominal conditions in Table 1 (acrylic IOL) and Figures 3, B, and 4A, with a 2.6-degree shadow located temporally from RFAs of 85.7 to 88.3 degrees. The other images come from the graphs in Figure 4A, in which the length of a vertical slice of the shaded area would be the width of the shadow and the corresponding red points and blue points, the RFA locations. All the factors increasing the risk for negative dysphotopsia would increase the width of the shadow. The location, however, is more complex and depends on the other variables. For example, from Figure 4A it can be seen that as the axial separation becomes shorter or angle  $\kappa$  increases, the RFAs become larger and thus the location becomes more peripheral. From Figure 4A it is clear that unless angle  $\kappa$  is

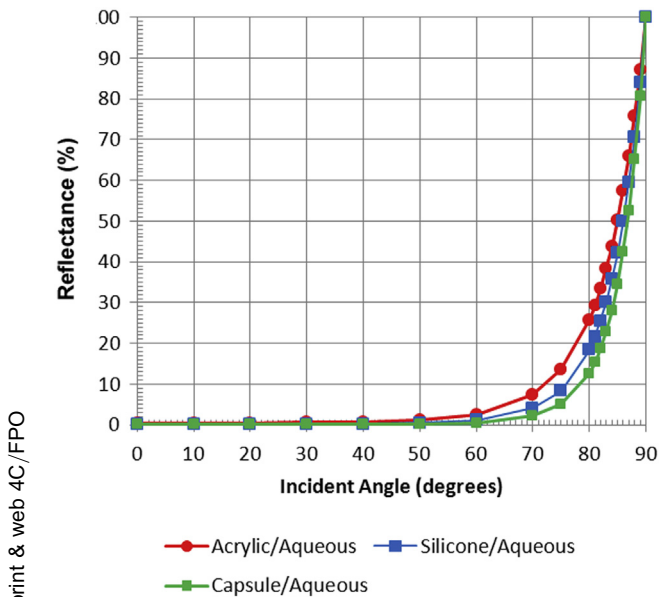


**Figure 6.** Reflectance curves for aqueous–acrylic (1.336, 1.550), aqueous–silicone (1.336, 1.460), and aqueous–capsule (1.336, 1.413 Gullstrand's). The amount of light reflected by the IOL would be in excess of 90% for the maximum limiting refracted ray leaving less than 10% actually transmitted. If the capsule is in the light path, the light transmitted through the capsule is less than 1%. Removal of nasal capsule overlying the anterior IOL surface has been shown to reduce or eliminate negative dysphotopsia.

considered, the axial position of the IOL would not correlate with the presence of negative dysphotopsia, as found clinically by Vámosi et al.<sup>19</sup>

The mean angle  $\kappa$  is 3.0 degrees  $\pm$  0.13 (SD) (higher for hyperopia and lower for myopia); therefore, values above

## FACTORS

### Primary

- Smaller photopic pupil
- Larger positive angle  $\kappa$
- Shape of IOL (with steeper posterior surface)
- Smaller axial distance of IOL behind iris
- Nasal anterior capsule overlying anterior nasal IOL
- Higher dioptric power if equi-biconvex or plano-convex
- Optic–haptic junction of IOL not horizontal (or superonasal by 30°)

### Secondary

- Edge design (truncated versus rounded and thickness)
- Material of IOL (higher versus lower index)
- Negative aspheric surface(s)

**Figure 8.** Factors increasing risk for negative dysphotopsia in order of importance ( $\kappa$  = angle kappa; IOL = intraocular lens).

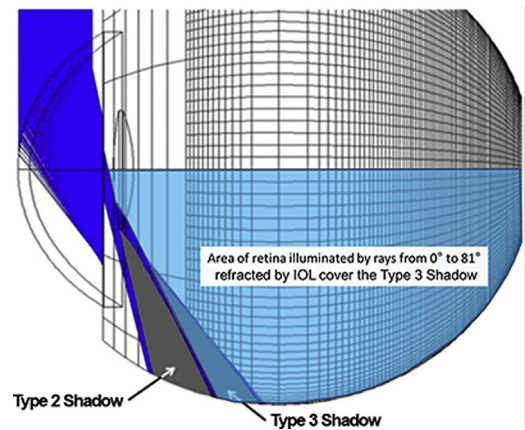


**Figure 7.** Ray trace of type 3 shadow, modified from Holladay et al.,<sup>3</sup> where the ray forming the anterior border of the type 3 shadow originates from an angle of 81.0 degrees to the optical axis passing through the nasal posterior surface of the IOL and the posterior ray from 93.4 degrees to the nasal edge of the shadow between shown on the retina. However, when rays from smaller angles passing through the lens (0 to 81 degrees) are added, as occurs in natural conditions, they completely cover the type 3 shadow, as shown in the figure (IOL = intraocular lens).

3.26 degrees (mean + 2 SD) would be considered abnormally high.<sup>6</sup> Current optical biometers and topographers report chord length  $\kappa$  (approximation of angle  $\kappa$ ); however, this value is given in millimeters (or microns) and is referred to as the pupil barycenter.<sup>20</sup> A standard approximation conversion of 1.0 mm to 7.5 degrees can be used when measured along the surface of the cornea<sup>21</sup>; thus, chord length values above 0.44 mm (3.26 degrees/7.5 degrees) are abnormally high. Patients with a chord length  $\kappa$  of 0.44 mm or higher would be at an increasingly higher risk for negative dysphotopsia, as has also been found for halos and glare with diffractive multifocal IOLs.<sup>22,23</sup>

Using a convex-plano optic IOL should reduce the risk for negative dysphotopsia; however, the complex interplay of factors shown in Figure 8, some of which the surgeon cannot control, can never eliminate the possibility of negative dysphotopsia. Clinical evaluations of negative dysphotopsia have typically not reported all the parameters in Figure 8 because at the time they were not known to be important. The horizontal VFA at which the shadow is most prominent and the angular width of the shadow have not previously been reported. Figure 4 indicates that the location would be from 80 to 105 degrees RFA and the width from near zero (*dark vertical line*) to 6 degrees (maximum horizontal width of shadow temporally). The methods in this paper now provide a framework for evaluating the eye parameters in detail.

It is also evident that the effect of larger diameter IOLs (oval or round) would not necessarily reduce or eliminate the gap, as has been found clinically,<sup>24</sup> because a larger diameter IOL would affect the missing and refracted rays similarly and move the gap, but not necessarily reduce it. This might also be a factor in why secondary piggyback IOLs are not always successful in eliminating or reducing

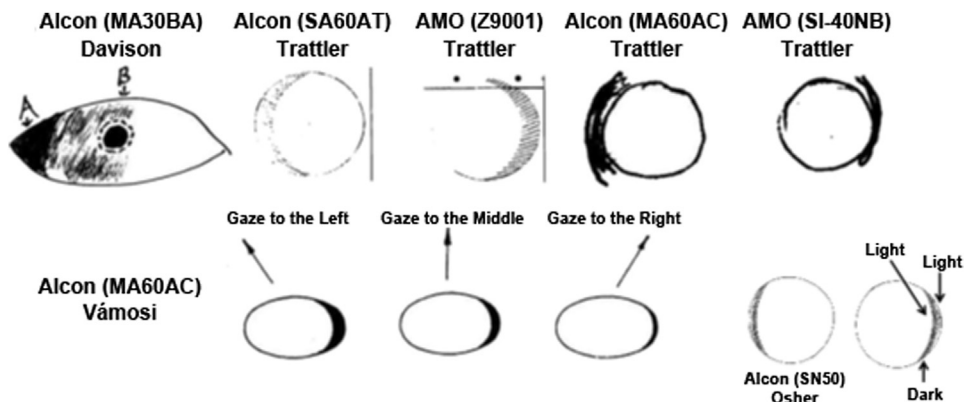


**Figure 9.** Patient drawings of negative dysphotopsia. Note that in the *bottom right* corner, the patient draws an extreme temporal lighted crescent, a dark crescent shadow, and then light area back to the fovea. The extreme temporal lighted crescent is from the rays that miss the IOL (Figure 3, C). (Copyright © Elsevier Inc. Reprinted with permission).

negative dysphotopsia because the effect on the refracted rays and missing rays is similar.

In our model, we have considered the optic of the IOL to be circular and the minimum ray missing the IOL to be limited by the nasal pupil and nasal edge of the optic of the IOL. This is true for 3-piece IOLs but is not true for 1-piece IOLs or plate-haptic IOLs. In these latter IOLs, if the IOL is oriented so that the optic-haptic junctions are placed horizontally (3 o'clock and 9 o'clock), the limiting ray missing the optic will pass through the haptic of the IOL.

Simple haptics (surfaces are parallel) do not deviate the ray but rather displace the ray posteriorly by an amount that depends on the thickness and index of refraction of the haptic and the angle of incidence of the ray.<sup>25</sup> Refraction by a simple haptic will displace posteriorly the minimum limiting ray just missing the optic by approximately one

half the thickness of the haptic, which can reduce or eliminate the shadow on the retina.

In our presentation on dysphotopsia at the American Society of Cataract and Refractive Surgery Cornea Day,<sup>A</sup> we proposed that a 1-piece IOL should be rotated such that the shoulders (optic-haptic junctions) are exactly horizontal. This was a result of an observation by Stulting<sup>B</sup> that negative dysphotopsia was reduced with this orientation.<sup>3</sup> Henderson et al.<sup>26</sup> have performed an excellent clinical study in which they placed the optic-haptic junction at 30 degrees in right eyes (2 o'clock and 8 o'clock) and at 150 degrees in left eyes (10 o'clock and 4 o'clock), reducing the incidence of negative dysphotopsia by 2.3 on day 1. However, the mechanism is not from "blocking the light" as they suggest because the haptic refracts incident light. Also, it is not the inferotemporal

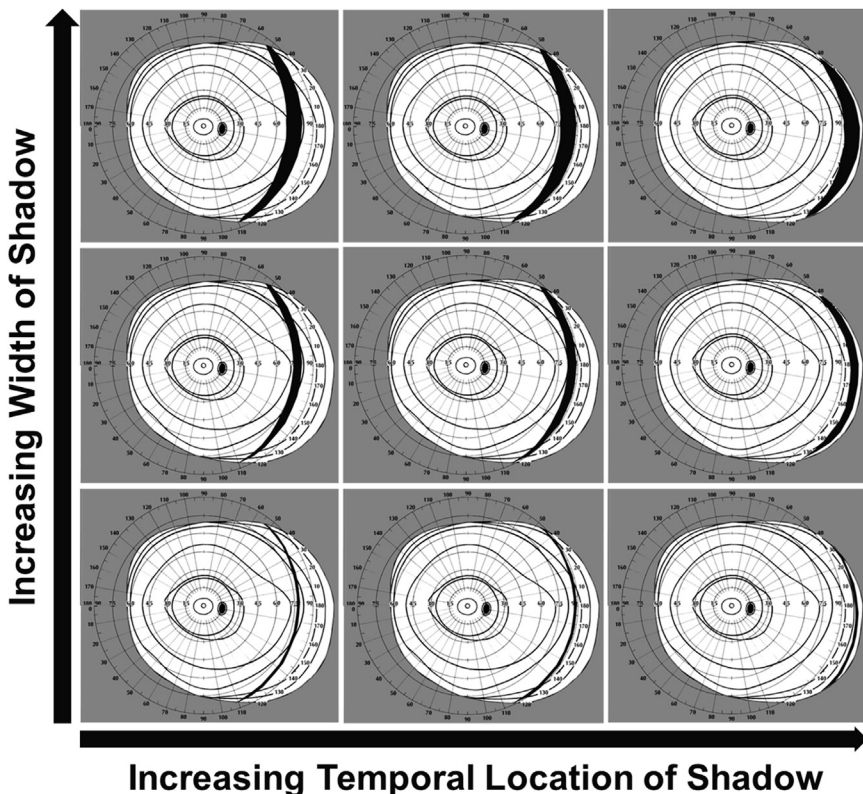


**Figure 10.** Simulated retinal images of shadows with varying width and temporal location for a 2.5 mm pupil. The central image represents the nominal conditions in Table 1 (acrylic IOL) and Figures 3, B, and 4A with a 2.6-degree shadow located temporally from RFAs of 85.7 to 88.3 degrees. The other images come from the graphs in Figure 4A, where the length of a vertical slice of the shaded area would be the width of the shadow and the corresponding *red* and *blue* points the RFA locations. All factors increasing the risk for negative dysphotopsia would increase the width of the shadow. The location, however, is more complex and depends on each parameter. For example, from Figure 4A it can be seen that as the axial distance becomes shorter or angle  $\kappa$  increases, the location (RFAs) become larger and thus the location becomes more peripheral.

haptic (4 o'clock or 8 o'clock) that reduces negative dysphotopsia but the superonasal haptic (2 o'clock or 10 o'clock) reducing the shadow on the superonasal retina (inferonasal visual field). In Figure 10, it is apparent that the temporal field is larger inferiorly than superiorly so that aligning the nasal optic–haptic junction slightly superiorly (up to 30 degrees or 1 clock hour) might be preferable to horizontal. However, this will require further study.

We also evaluated the visual field in pseudophakia in terms of a double retinal image and constriction. For the 2.5 mm pupil, Figures 3 and 4A show the ray-tracing calculations for our nominal acrylic IOL; note the slight gap between the refracted rays and the missing rays, which would result in the perception of a shadow. The retinal image in the far periphery of the pseudophakic eye (Figure 3, B and C) is different from the image formed in the phakic eye (Figure 3, A). For the 2.5 mm pupil (Figure 2, left), pseudophakic VFAs from 83.8 to 97 degrees (blue area) are imaged at 2 different locations on the retina because a portion of the light is refracted by the IOL (blue curve) and the remainder of the light misses the IOL (red curve). The double retinal image might appear to be continuous to the observer if there is an overlap of these 2 retinal images because the peripheral retina is so low in resolution (counting fingers at a few feet).<sup>8</sup>

The ray-tracing analysis also showed that the pseudophakic maximum VFA is slightly constricted (Figure 2, red area) to 104 degrees compared with 109 degrees in the phakic eye. There will always be rays that miss the IOL if there is a space between the iris and IOL, and these rays missing the IOL are the only source of VFAs above 97 degrees.

In Figure 3, C, it is apparent that most rays missing the IOL must pass through the peripheral capsule and only a small portion of the rays would pass through the zonular space, which decreases or disappears with time postoperatively.<sup>27</sup> In the early postoperative period, the capsule appears clear and the resulting image on the retina would be somewhat out of focus depending on the IOL shape (Figure 5); however, a shadow (or gap) would still be distinct. The rays on the peripheral capsule are still oblique, but at significantly smaller angles (~65 degrees) than those on the anterior capsule overlying the IOL (near 90 degrees) because of the curvature of the anterior IOL surface and the larger VFA. As seen in Figure 6, at incident angles of less than 85 degrees, the vast majority of light is transmitted. With time, the lens epithelial cells (LECs) that lie under the anterior and equatorial lens capsule<sup>28,29</sup> begin the process of opacification (become translucent), which would cause significant forward lightscatter.<sup>30–32</sup> In the vast majority of patients, the scattered light would fill the void (gap) that causes negative dysphotopsia, explaining the 84% reduction in negative dysphotopsia by the second to third year after surgery.<sup>33</sup> However, the rate of opacification is quite variable and the area is patchy and unique to each patient; therefore, a window of clear nasal capsule could

remain, resulting in a few patients for whom negative dysphotopsia might never disappear.

There are limitations to our model. The human eye is much more complicated than our model. The corneal surfaces are not simple prolate surfaces but irregular,<sup>34</sup> the iris is not exactly orthogonal to the optical axis and has varying thickness,<sup>35</sup> IOLs are often decentered or tilted,<sup>35,36</sup> the retina is not a spherical or even an elliptical surface,<sup>11,37</sup> and only simple IOL edges and haptics were considered. Also, the IOL optical surfaces go to the lens edge, which is not always the case, in particular for lower refractive index materials. Nevertheless, the direction of the effect of the primary and secondary causative factors shown in Figure 8 will not change with more complicated models and the values in our models are only approximations that are useful for populations but not for specific eyes. In short, all patients matching the nominal parameters for an acrylic IOL in Table 2 would not have a 2.6-degree gap and consequent negative dysphotopsia. However, those with smaller pupils, higher angle  $\kappa$ 's and an equi-biconvex shaped IOL with negative asphericity, higher index of refraction, higher dioptric power, truncated edges, and anterior nasal capsule overlying the IOL are at higher risk.

Successful treatment of negative dysphotopsia requires eliminating the gap between the maximum refracted ray and the minimum ray missing the IOL optic, or moving the gap anteriorly beyond functional retina. Using a 1-piece or plate–haptic IOL and aligning the optic–haptic junction between horizontally<sup>3</sup> and 30 degrees superonasally<sup>26</sup> at the time of surgery is a preventative measure that will reduce the risk for negative dysphotopsia.

Removal of the anterior capsule in the nasal quadrant overlying the IOL is the simplest and safest first step to reduce or eliminate negative dysphotopsia and has been reported to be 60% successful.<sup>13–15</sup> Intraocular lens exchange in the sulcus<sup>38</sup> and secondary piggyback IOL implantation in the sulcus<sup>39</sup> position the IOL closer to the posterior iris, which would increase the minimum ray missing and the maximum ray refracted by the IOL. This will move the shadow farther peripherally but not necessarily beyond the functional retina. Results in Table 2 and Figure 5 suggest that a silicone convex-plano shaped IOL with a rounded edge might be a better choice. If the maximum pseudophakic ray is still posterior to the anterior limit of functional retina and does not overlap the minimum ray missing the IOL, the negative dysphotopsia will be reduced, but not eliminated. It can only be eliminated if the maximum refracted rays by the IOL are moved anterior to the limit of functional retina (nominal RFA of 109 degrees) or overlap the rays missing the IOL optic.

A rounded edge IOL<sup>40</sup> would increase the limiting anterior refracted ray by a few degrees; however, it would also eliminate the barrier to LECs, leading to an increase in posterior capsule opacification (PCO), which yields a substantial risk for complications when opening the posterior capsule. Reverse optic capture might move the IOL

anteriorly, which will move the possibility of a shadow more peripherally or eliminate it. It also has the same effect as removing the anterior nasal capsule and ensures that the anterior surface of the IOL is fully exposed and the capsule is not the limiting factor for nasal rays. However, it also increases the risk for PCO, whereas laser removal of the anterior capsule is safer and equally effective.

In summary, factors that increase the risk for negative dysphotopsia might be categorized as patient characteristics (small photopic pupil, high angle  $\kappa$ , and hyperopia), IOL design (equi-biconvex, high dioptric power, high index of refraction, negatively aspheric, and truncated edges), and surgical technique (uniform overlap of the nasal edge of the IOL by anterior capsule<sup>41</sup> and orientation of optic-haptic junction not between horizontal and superonasal). In the decade before Davison's first report of negative dysphotopsia,<sup>1</sup> IOL designs and surgical techniques that increase the risk for negative dysphotopsia were becoming more prevalent.

#### WHAT WAS KNOWN

- Negative dysphotopsia presents as a dark crescent-shaped shadow in the extreme temporal periphery.

#### WHAT THIS PAPER ADDS

- When light rays that miss the optic of the IOL are considered along with rays that are refracted, there can be a gap in the peripheral retinal image that corresponds to negative dysphotopsia.
- Ray tracing identified that the primary factors are smaller photopic pupil, larger angle  $\kappa$ , shape of the IOL, axial location and orientation of the IOL, and anterior capsule overlying anterior nasal IOL.
- Higher dioptric power equi-biconvex-shaped IOLs create a higher risk for negative dysphotopsia.
- There is a constriction and double retinal image of the extreme temporal visual field in pseudophakia.

#### REFERENCES

1. Davison JA. Positive and negative dysphotopsia in patients with acrylic intraocular lenses. *J Cataract Refract Surg* 2000; 26:1346–1355
2. Henderson BA, Geneva II. Negative dysphotopsia: a perfect storm. *J Cataract Refract Surg* 2015; 41:2291–2312
3. Holladay JT, Zhao H, Reisin CR. Negative dysphotopsia: the enigmatic penumbra. *J Cataract Refract Surg* 2012; 38:1251–1265. Available at: [http://www.hicsoap.com/publications/107%20Neg%20Dys%20FINAL%20PUB%20JCRS%20July%202012\\_38\\_1251-1265.pdf](http://www.hicsoap.com/publications/107%20Neg%20Dys%20FINAL%20PUB%20JCRS%20July%202012_38_1251-1265.pdf). Accessed December 27, 2016
4. Holladay JT. Reply to letter by S Masket and N Fram. Etiology of negative dysphotopsia. *J Cataract Refract Surg* 2013; 39:486.e1–486.e4
5. Liou HL, Brennan NA. Anatomically accurate, finite model eye for optical modeling. *J Opt Soc Am A* 1997; 14:1684–1695
6. Basmak H, Sahin A, Yildirim N, Papakostas TD, Kanellopoulos AJ. Measurement of angle kappa with synoptophore and Orbscan II in a normal population. *J Refract Surg* 2007; 23:456–460
7. Hartridge H. The limit to peripheral vision. Proceedings of the Physiological Society 1919. Published in *J Physiol* 1920; 53:xvii–xviii. Available at: <http://onlinelibrary.wiley.com/doi/10.1113/jphysiol.1920.sp001894/pdf>. Accessed December 26, 2017
8. Campbell CJ, Koester CJ, Rittler MC, Tackaberry RB. *Physiological Optics*. Hagerstown, MD, Harper & Row, 1974; chapter 7
9. Simpson MJ. Vignetting and negative dysphotopsia with intraocular lenses in “far peripheral vision”. *J Opt Soc Am A Opt Image Sci Vis* 2015; 32:1672–1677
10. Simpson MJ. Managing and understanding negative dysphotopsia [letter]. *J Cataract Refract Surg* 2015; 41:477; reply by TR Burke, L Benjamin, 478–479
11. Atchison DA, Markwell EL, Kasthurirangan S, Pope JM, Smith G, Swann PG. Age-related changes in optical and biometric characteristics of emmetropic eyes. *J Vis* 2008; 8 (4): 29, 1–20. Available at: <http://www.journalofvision.org/content/8/4/29.full.pdf>. Accessed December 27, 2016
12. Erb-Eigner K, Hirschall N, Hackl C, Schmidt C, Asbach P, Findl O. Predicting lens diameter: ocular biometry with high-resolution MRI. *Invest Ophthalmol Vis Sci* 2015; 56:6847–6854. Available at: <http://iovs.arvojournals.org/article.aspx?articleid=246680>. Accessed December 27, 2016
13. Folden DV. Neodymium:YAG laser anterior capsulectomy: surgical option in the management of negative dysphotopsia. *J Cataract Refract Surg* 2013; 39:1110–1115
14. Holladay JT. Cataract surgical problem. In: Masket S, ed, Consultation section. *J Cataract Refract Surg* 2013; 39:1125–1126
15. Michelson MA, Holladay JT. The intersection of optics and neuro-ophthalmology: the enigma of pseudophakic dysphotopsia. *J Neuro-Ophthalmol* 2015; 35:109–111
16. Makhotkina NY, Berendschot TT, Nuijts RM. Objective evaluation of negative dysphotopsia with Goldmann kinetic perimetry. *J Cataract Refract Surg* 2016; 42:1626–1633
17. Linke SJ, Baviera J, Munzer G, Fricke OH, Richard G, Katz T. Mesopic pupil size in a refractive surgery population (13,959 eyes). *Optom Vis Sci* 2012; 89:1156–1164
18. Cakmak HB, Cagil N, Simavlıo H, Duzen B, Simsek S. Refractive error may influence mesopic pupil size. *Curr Eye Res* 2010; 35:130–136
19. Vámosi P, Csákány B, Németh J. Intraocular lens exchange in patients with negative dysphotopsia symptoms. *J Cataract Refract Surg* 2010; 36:418–424
20. Chang DH, Waring GO IV. The subject-fixated coaxially sighted corneal light reflex: a clinical marker for centration of refractive treatments and devices. *Am J Ophthalmol* 2014; 158:863–874
21. Brodie SE. Photographic calibration of the Hirschberg test. *Invest Ophthalmol Vis Sci* 1987; 28:736–742. Available at: <http://iovs.arvojournals.org/article.aspx?articleid=2177798>. Accessed December 27, 2016
22. Prakash G, Prakash DR, Agarwal A, Kumar DA, Agarwal A, Jacob S. Predictive factor and kappa angle analysis for visual satisfactions in patients with multifocal IOL implantation. *Eye* 2011; 25:1187–1193. Available at: <http://www.ncbi.nlm.nih.gov/pmc/articles/PMC3178249/pdf/eye2011150a.pdf>. Accessed December 27, 2016
23. Karhanová M, Marešová K, Pluhacek F, Mlčak P, Vlácil O, Són M. [The importance of angle kappa for centration of multifocal intraocular lenses]. [Czechoslovakian]. *Cesk Slov Oftalmol* 2013; 69:64–68
24. Masket S, Rubin D, Fram NR. Dysphotopsia and oval intraocular lenses. *J Cataract Refract Surg* 2016; 42:635–636
25. Michaels DD. *Visual Optics and Refraction: A Clinical Approach*, 3rd ed. St. Louis, MO, CV Mosby, 1985; 30
26. Henderson BA, Yi DH, Constantine JB, Geneva II. New preventative approach for negative dysphotopsia. *J Cataract Refract Surg* 2016; 42:1449–1455
27. Modesti M, Pasqualitto G, Appolloni R, Pecorella I, Sourdille P. Preoperative and postoperative size and movements of the lens capsular bag: ultrasound biomicroscopy analysis. *J Cataract Refract Surg* 2011; 37:1775–1784
28. Humphry RC, Davies EG, Jacob TJC, Thompson GM. The human anterior lens capsule—an attempted chemical debriement of epithelial cells by ethylenediaminetetraacetic acid (EDTA) and trypsin. *Br J Ophthalmol* 1988; 72:406–408. Available at: <http://www.ncbi.nlm.nih.gov/pmc/articles/PMC1041470/pdf/brjophthal00610-0007.pdf>. Accessed December 27, 2016
29. Hogan MJ, Alvarado JA, Weddell JE. *Histology of the Human Eye; An Atlas and Textbook*. Philadelphia, Saunders, 1971; Chapters 6 and 12
30. Witmer FK, van den Brom HJB, Kooijman AC, Blanksma LJ. Intra-ocular light scatter in pseudophakia. *Doc Ophthalmol* 1989; 72:335–340
31. Smith SR, Daynes T, Hinckley M, Wallin TR, Olson RJ. The effect of lens edge design versus anterior capsule overlap on posterior capsule opacification. *Am J Ophthalmol* 2004; 138:521–526
32. Sacu S, Menapace R, Findl O, Georgopoulos M, Buehl W, Kriechbaum K, Rainer G. Influence of optic edge design and anterior capsule polishing on posterior capsule fibrosis. *J Cataract Refract Surg* 2004; 30:658–662
33. Osher RH. Negative dysphotopsia: long-term study and possible explanation for transient symptoms. *J Cataract Refract Surg* 2008; 34:1699–1707
34. Dubbelman M, Sicam VA, van der Heijde GL. The shape of the anterior and posterior surface of the aging human cornea. *Vision Res* 2006; 46:993–1001

35. Nishi Y, Hirschall N, Crnej A, Gangwani V, Tabernero J, Artal P, Findl O. Reproducibility of intraocular lens decentration and tilt measurement using a clinical Purkinje meter. *J Cataract Refract Surg* 2010; 36:1529–1535
36. Rosales P, De Castro A, Jiménez-Alfaro I, Marcos S. Intraocular lens alignment from Purkinje and Scheimpflug imaging. *Clin Exp Optom* 2010; 93:400–408. Available at: <http://onlinelibrary.wiley.com/doi/10.1111/j.1444-0938.2010.00514.x/epdf>. Accessed December 27, 2016
37. Atchison DA, Pritchard N, Schmid KL, Scott DH, Jones CE, James M, Pope JM. Shape of the retinal surface in emmetropia and myopia. *Invest Ophthalmol Vis Sci* 2005; 46:2698–2707. Available at: <http://iovs.arvo-journals.org/article.aspx?articleid=2182758>. Accessed December 27, 2016
38. Vámosi P. Cataract surgical problem. In: Masket S, ed, Consultation section. *J Cataract Refract Surg* 2013; 39:1126
39. Burke TR, Benjamin L. Sulcus-fixated intraocular lens implantation for the management of negative dysphotopsia. *J Cataract Refract Surg* 2014; 40:1469–1472
40. Weinstein A. Cataract surgical problem. In: Masket S, ed, Consultation section. *J Cataract Refract Surg* 2013; 39:1125
41. Capsule stabilization for phacoemulsification [letter]. *J Cataract Refract Surg* 2000; 26:629; reply by P Bloom, V Lee, 629

#### OTHER CITED MATERIAL

- A. Holladay JT, "Management of Dysphotopsias following Cataract Surgery," presented on Cornea day at the ASCRS Symposium on Cataract, IOL and Refractive Surgery, April 2014
- B. Stulting RD, personal communication, November 2011

**Disclosure:** *Neither author has financial or proprietary interest in any material or method mentioned.*



#### First author:

Jack T. Holladay MD, MSEE

*Department of Ophthalmology, Baylor College of Medicine, Houston, Texas, USA*